Evaluation of the acoustic radiation of contrasted orthogonally stiffened plates from homogenized model

Pascal Fossat, Thomas Brion, Mohamed Ichchou, Olivier Bareille

Evaluation of the acoustic radiation of contrasted orthogonally stiffened plates from homogenized model

Pascal Fossat[a,*], Thomas Brion[a], Mohamed Ichchou[a], Olivier Bareille[a]

[a] *Vibroacoustics and Complex Media Research Group VIAME, LTDS - CNRS UMR 5513, Centre Lyonnais d'Acoustique CeLyA, École Centrale de Lyon, Université de Lyon, France*

Abstract

This paper presents a study of the acoustic radiation from a ribbed plate with inner resonance. Based on explicit design rules and homogenized model for flexural waves, it reminds that bending wave propagation significantly differs from classical models in case of strong contrast between constituents, resulting into inner resonance. In order to demonstrate that this model advantageously supplements the Timoshenko orthotropic plate model, it links the atypical structural response on common vibroacoustic indicators, which are of value to discuss on different levels of abstraction. In either infinite or finite cases, the resulting indicators obtained from the homogenized model matches with classical trends outside frequency bands associated with local resonance, however inner resonance yields additional frequency ranges in which acoustic radiation is either strongly reduced or enhanced. For both mechanical and acoustic quantities, key indicators are successfully compared with classical theory for either poorly and highly contrasted ribbed plates in order to confirm the diversification of acoustic behaviors encompassed by the homogenized model.

Keywords: Homogenization, Contrasted structure, Ribbed plate, Inner resonance media, Acoustic radiation, Sound transmission loss

*Corresponding author
Email address: pascal.fossat@ec-lyon.fr (Pascal Fossat)

Highlights

- Homogenized model of ribbed plates discussed versus Timoshenko orthotropic model
- Benefit of homogenized model over classical model for highly contrasted plates
- Theoretical influence of the locally resonant behavior on vibroacoustic indicators

Introduction

The use of ribbed panels in aerospace or automotive engineering is wide and the current trends associated with sound and vibration control have been a vector of development of new models and methods. Indeed the coupled problem of a vibrating plate in a fluid medium is related to fluid-structure interaction for which assumptions can be made either on the dynamic behavior of the plate, the properties of the fluid governing the radiated field, the nature of the coupling between the plate and the fluid.

The acoustic field radiated by a plate is known from its vibratory response [1, 2]. The simple case of an infinite thin isotropic plate radiating in an infinite fluid domain shows the existence of a critical frequency below which the plate vibrates without radiating acoustic waves (subsonic regime with evanescent waves), and above which the plate radiates plane waves whose direction of propagation depends on the frequency (supersonic regime). While the infinite case has some analytical solutions for both regimes, the determination of the acoustic field radiated in finite case requires the implementation of the Rayleigh integral based on the Green kernel available for given set of geometries. It is outlined that although the structural response of the plate can be determined or approached analytically using Rayleigh-Ritz method, virtual works principle, or by finite element or finite difference schemes, the acoustical response is only accessible through the resolution of the Rayleigh integral, that might be computationally expensive. For a complete review of structure-borne acoustics of rectangular panels and comprehensive review of numerical techniques to assess the low frequency radiation, one may respectively refer to the papers from [3, 4]. This overview of methods provides a reading grid for various experimental works in the scope of this paper, such as those of [5, 6].

A key point of this paper is the aspect of contrast, which can be either geometric or mechanical in nature. The modeling of this specific feature modifies the structure of the bi-laplacian operator (classical Kirchhoff's description) by introducing additional bending stiffness coefficients associated with orthotropy. The most common model for orthotropic plate was developed by Timoshenko [7] and applies to unidirectionally and orthogonally ribbed plates, beam grids, corrugated plates through the calculation of equivalent bending stiffness terms.

Focusing on ribbed plates, for which the orthotropic nature arises from the arrangement of stiffeners on a bare plate, it appears that the stiffeners

significantly affect its dynamic characteristics. One must cite the pioneering works of [8] who demonstrated that the radiation efficiency is increased below the critical frequency by assuming stiffeners as regularly spaced supports. A physical interpretation was introduced later in [9] and describes how the ribs may bring wavenumbers from the subsonic regime to the supersonic regime. Among the different theories to describe the dynamic behavior of periodic stiffened panel, one may refer to the wavenumber based method [10], the space-harmonic analysis [11], wave finite element method [12–14], and some analytical approaches [15–17], among which homogenization is a relevant theoretical framework for the construction of analytical models.

However, most of these works consider structures in which the mechanical properties of the constituents are poorly contrasted. Particularly, these studies give either analytical results on weakly contrasted structures, or numerical results on contrasted structures.

Among the analytical approaches, a benefit of periodic homogenization is to upscale the physics from to micro-scale to the macro-scale without assumption about the nature of the model to be found [18]. Also, giving that the resonant nature at the macroscopic scale comes from the contrast between the constituents, the transition from weakly to strongly contrasted, *i.e.* non-resonant to resonant, can be assessed. Indeed, the asymptotic homogenization is capable of precisely describe this transition of behavior through the scaling of geometrical and mechanical contrasts directly into the derivation process. In this way, on may cite the derivation of models of contrasted frames [19], plate-type structures such as laminated plates [20, 21], unidirectional ribbed plate [22], and orthogonally ribbed plates [23].

Although this analytical method is intrinsically limited to low frequencies, it is sufficient to capture the first eigenmodes of the structure while incorporating the effect of local resonance. As an example, the locally resonant nature of an infinite unidirectional ribbed plate was briefly introduced in [24] and showed that it brings additional frequency bands of radiation below the critical frequency, as well as evanescent waves below the critical frequency. Also, explicit design rules could allow to tune local resonance onto the coincidence frequency as in [25] and thus make it possible to reach improved sound insulation as already known for locally resonant mechanical or acoustical metamaterials, and recently demonstrated by [26–28].

Although numerous study bring meaningful phenomenological interpretations on the radiation of resonant panels, only little attention has been paid to draw a parallel between an analytical model of contrasted ribbed and its

acoustic radiation compared to classical model.

In this paper, the acoustic radiation of a contrasted orthotropic plate is reported in the infinite case and finite case. The paper is organized into three sections. A preliminary description of the structure under study is introduced in section 1, together with the underlying physics and associated mechanisms. The models introduced will be exploited in the case of an infinite plate, then of finite dimensions. Particularly, section 2 presents the outputs of the model on common vibroacoustic indicators such as radiation efficiency, acoustic impedance, and transmission loss. The section 3 deals with finite plate analysis, and compares the response of the contrasted model with that of Timoshenko, in terms of mean square velocity and sound transmission loss.

1. Physical insight of ribbed plate models

1.1. Structure under study

The periodic orthogonally ribbed plate hereafter called 2D-ribbed plates under study is depicted in Fig. 1. It comprises identical "micro"-plate elements (denoted $\mathcal{P}$) connected to an orthogonal beam grid (denoted $\mathcal{G}$), both made of isotropic elastic materials. The beams of the grid are assumed significantly stiffer than the internal plates. We focus on the dynamic range such that the size of the cell (or the width of $\mathcal{P}$) is small compared to the wavelength in the beam grid. The referential frame of unit vectors $(\mathbf{e_x}, \mathbf{e_y}, \mathbf{e_z})$ is such that $\mathbf{e_x}$ and $\mathbf{e_y}$ are the in-plane vectors along the orthogonal ribs, while $\mathbf{e_z}$ is the out-of-plane vector. The beam grid $\mathcal{G}$ is defined by perpendicular beams. The stiffeners oriented along x (resp. y) are identical and regularly spaced by the length ℓ_y (resp. ℓ_x).

Each segment of stiffeners between two consecutive nodes is modeled as an Euler-Bernoulli beam (denoted $\mathcal{B}_x$, $\mathcal{B}_y$). The geometrical parameters of $\mathcal{B}_j$, with $j = x, y$, are (ℓ_j, h_j, b_j, A_j) which stand respectively for their length, $\mathbf{e_z}$-thickness, width with $b_j = O(h_j)$ and section area $A_j = h_j b_j$. The mechanical parameters $(E_j, I_j = b_j h_j^3/12, G_j, \mathcal{I}_j, \rho_j, \Lambda_j = \rho_j A_j, \rho_j J_j)$ denote respectively the Young Modulus, the bending inertia, the torsional modulus and torsional inertia, the density, the linear mass, and the polar moment. The dimensions of the sections $\sqrt{A_j}$ are assumed small with respect to the lengths ℓ_j so that the behavior of the inter-node elements can be effectively modeled as Euler-Bernoulli beams. It is further assumed that the geometrical and the

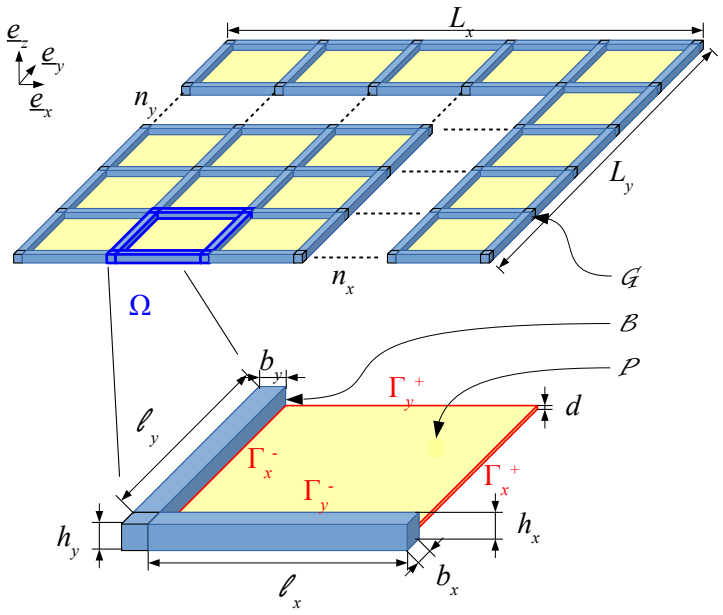

Figure 1: Orthogonally ribbed plate with with beams constituting the beam grid $\mathcal{G}$, and focus on the unit cell Ω made of micro-beams $\mathcal{B}$ and internal micro-plate $\mathcal{P}$

mechanical parameters of both types of beams $\mathcal{B}_j$ are of the same order of magnitude.

The material of the micro-plates $\mathcal{P}$ of area $\ell_x \ell_y$ and thickness d, have a Young's modulus E_p, a Poisson's ratio ν_p and a density ρ_p. The corrected plate modulus is $E'_p = E_p/(1-\nu_p^2)$. The plate bending inertia is denoted $I'_p = d^3/12$ and the surface mass $\Lambda'_p = \rho_p d$.

According to the ribbed plate illustrated in Fig. 1, two models are presented in the following : a poorly contrasted ribbed plate in section 1.2 and a highly contrasted plate model in section 1.3.

1.2. Summary of the 2D ribbed plate model without contrasts

As introduced previously, numerous studies dealing with orthogonally ribbed plates are based on Timoshenko description [7]. This description is originally given in statics and is commonly extended in the dynamic regime

by introducing $-\omega^2 \Lambda u$ on the right hand side of the equation. For an orthotropic plate defined in the (x, y) plane, the equation governing its transverse displacement u takes the form of Eq. (1) with coefficients Eq. (2).

$$\left(D_x \frac{\partial^4}{\partial x^4} + D_y \frac{\partial^4}{\partial y^4} + 2 D_{xy} \frac{\partial^4}{\partial x^2 \partial y^2} \right) u = \omega^2 \Lambda u \tag{1}$$

where the bending rigidities and mass are

$$D_x = \frac{E_x I_x}{l_y} + E'_p I_p \; ; \; D_y = \frac{E_y I_y}{l_x} + E'_p I_p \; ; \; D_{xy} = E'_p I_p \; ; \; \Lambda = \frac{\Lambda_x}{\ell_y} + \frac{\Lambda_y}{\ell_x} + \Lambda'_p \tag{2}$$

From the original description in statics, the expressions of respective bending stiffness suggest that the plate contributes to the global rigidity of the plate. This is understood since same order of magnitude, one cannot neglect the effect of the plate to the beam grid. Also, introducing $-\omega^2 \Lambda u$ on the right hand side of the equation without prior investigation might not be fully appropriated to capture all the frequency dependent phenomena.

Moving to the case of contrasted plate would require a decoupling of the beam grid and the plate, so that contrast is introduced in the plate either with geometrical or mechanical parameters. The next section introduces the contrast between the beam grid and the internal plates, and discusses how contrast enriches Timoshenko description.

1.3. Summary of the homogenized ribbed plate model with contrasts

This subsection defines favorable conditions for inner resonance and summarizes the derivation of the homogenized model. The homogenization process is carried out according to the following steps : *i*) the homogenization of periodic discrete media method enables to derive the dynamic model describing the transverse vibration of the beam grid only, *ii*) the coupling between the beam grid and the internal plates is then introduced considering that the grid is loaded by efforts and moments exerted by the plates attached to it, *iii*) the calculation of the dynamic contribution of the resonant internal plates driven by the motion of the grid.

1.3.1. Contrasts definition and design rules

Inner resonance is defined so as the stiff orthogonal beam grid conveys the large wavelength, while the soft internal plate experiences a local resonance. Such a mixed regime within the cell results into *i*) an inhomogeneous

kinematics where the plate and grid displacements differ at the leading order and *ii*) an asymmetrical coupling where the grid forces the soft plate.

First, as for the co-dynamic condition, the beam grid $\mathcal{G}$ and $\mathcal{P}$-plate fundamental resonances are of same order i.e., $O(\omega_{\mathcal{G}}) = O(\omega_p)$, so that :

$$O\left(\frac{E'_p I'_p}{\Lambda'_p \ell^4}\right) = O\left(\frac{EI}{\Lambda L^4}\right) \qquad \text{i.e.} \qquad \frac{E'_p}{E}\frac{\rho}{\rho_p} = O\left(\frac{h^2}{d^2}\frac{\ell^4}{L^4}\right) = O\left(\varepsilon^4 \frac{h^2}{d^2}\right) \quad (3)$$

This relation highlights the significant contrasts of mechanical properties of the constituting materials of the beam grid $\mathcal{G}$ and $\mathcal{P}$-plate.

Second, as for the asymmetric coupling, the grid acts as the forcing system that imposes its displacement to the internal plate which bring forces back on the grid. Such a coupling between the transverse balance of the grid loaded by the internal plates requires :

$$\mathrm{div}(\mathbf{T}_{\mathcal{G}}) = O(T_p) \quad (4)$$

where $\mathbf{T}_{\mathcal{G}}$ relates to the transverse shear force (unit kN) in the grid $\mathcal{G}$ and T_p is the transverse linear shear force in the internal $\mathcal{P}$-plate (unit kN/m).

Thus, from Eq. (4) and recalling that $b_k = O(h_k)$ one deduces the following requirement

$$O\left(E\frac{bh^3}{L^4}\right) = O\left(E'_p \frac{d^3}{\ell^3}\right) \qquad \text{i.e.} \qquad \frac{E'_p}{E} = O\left(\frac{\ell^3}{d^3}\frac{\ell^4}{L^4}\right) = O\left(\varepsilon^4 \frac{h^2}{d^2}\right) \quad (5)$$

In practice, $\rho/\rho_p = O(1)$ and the two conditions Eq. (3) and Eq. (5) reduce to $\frac{E'_p}{E} = O\left(\varepsilon^4 \frac{h^2}{d^2}\right)$. For ribbed plate made of a single material $E'_p = E$, and the inner-resonance arises when $d/h = O(\ell^2/L^2)$, i.e. for plates $\mathcal{P}$ significantly thinner than the beams of the grid $\mathcal{G}$. If the plates material is much softer that the grid material, namely $E'_p = O(\varepsilon^4 E)$ then $d/h = O(\ell/L)$ enables the inner-resonance to occur. Note that in these realistic cases, the bending stiffness of the plate is much smaller than that of the grid, in accordance with the asymmetry of the coupling. The case of inverted material properties so that the plate exhibits stiff properties and beam grid soft properties is not assessed here.

1.3.2. Homogenized formulation of the flexural behavior

Starting with the beam grid, the up-scaling process is performed through HPDM method (namely Homogenization of Periodic Discrete Media). The

developments proceed into three steps, namely, the discretization of the dynamic balance, then the homogenization procedure itself through scale separation assumption and normalization, leading to the continuous model from the discrete pattern. This method applies under the key assumption of scale separation. This means that the wavelength $O(L)$ is much larger than the period size $O(l)$ and consequently $\epsilon = l/L << 1$. The macroscopic description of the grid, valid at the dominant order, is the limit behavior reached for $\varepsilon = \ell/L \to 0$. After these few steps, we are left with the following macroscopic description of the grid at the leading order :

$$\begin{cases} \operatorname{div}(\mathbf{T}^{\mathcal{G}}) + \omega^2 \Lambda^{\mathcal{G}} u = 0 \qquad ; \qquad \Lambda^{\mathcal{G}} = \dfrac{\Lambda_x}{\ell_y} + \dfrac{\Lambda_y}{\ell_x} \\ \operatorname{div}(\mathbf{M}^{\mathcal{G}}) - \mathbf{T}^{\mathcal{G}} - \omega^2 \mathbf{J}^{\mathcal{G}}.\mathbf{grad}(u) = 0 \\ \\ \mathbf{M}^{\mathcal{G}} = -\begin{pmatrix} \frac{E_x I_x}{\ell_y}\partial_x^2 u & \frac{G_y J_y}{\ell_x}\partial_x\partial_y u \\ \frac{G_x J_x}{\ell_y}\partial_y\partial_x u & \frac{E_y I_y}{\ell_x}\partial_y^2 u \end{pmatrix} \qquad ; \qquad \mathbf{J}^{\mathcal{G}} = \begin{pmatrix} \rho_y J_y & 0 \\ 0 & \rho_x J_x \end{pmatrix} \end{cases} \tag{6}$$

The governing equation Eq. (6) may be written under condensed form

$$\frac{E_x I_x}{\ell_y}\frac{\partial^4 u}{\partial x^4} + \frac{E_y I_y}{\ell_x}\frac{\partial^4 u}{\partial y^4} + \left(\frac{G_x \mathcal{I}_x}{\ell_y} + \frac{G_y \mathcal{I}_y}{\ell_x}\right)\frac{\partial^4 u}{\partial x^2 \partial y^2} + \omega^2\left(\frac{\rho_y J_y}{\ell_x}\frac{\partial^2 u}{\partial x^2} + \frac{\rho_x J_x}{\ell_y}\frac{\partial^2 u}{\partial y^2}\right) = \omega^2\left(\frac{\Lambda_x}{\ell_y} + \frac{\Lambda_y}{\ell_x}\right)u \tag{7}$$

The governing equation Eq. (6) shows the coupling between the flexural and torsional behaviors. Note that in statics ($\omega \to 0$), this model already differs to that of Timoshenko Eq. (1). Note also that the inertial term containing the polar moments $\mathbf{J}^{\mathcal{G}}$ may be neglected in regards to those related to the linear masses $\Lambda^{\mathcal{G}}$. Note finally that an additional inertial effect following comment made in section 1.2.

The action of internal plates is than introduced in the beam grid model in the form an external loading constituted by a shear force $\mathcal{F}$ and a couple $\mathcal{C}$ resulting from the contact forces. The rigorous calculation of these terms is detailed in [23]. Calculating analytically these terms yield the effective model of the 2D ribbed plate that describes the grid behavior enriched by

for the locally resonant internal plates:

$$\begin{cases} \mathrm{div}(\mathbf{T}^{\mathcal{G}}) + \omega^2(\Lambda^{\mathcal{G}} + \Lambda'_p\langle\phi_\omega\rangle)u = 0 \\ \mathrm{div}(\mathbf{M}^{\mathcal{G}}) - \mathbf{T}^{\mathcal{G}} - \omega^2\mathbf{J}^{\mathcal{G}}.\mathbf{grad}(u) = 0 \end{cases} \tag{8}$$

with $\mathbf{M}^{\mathcal{G}}$ and $\mathbf{J}^{\mathcal{G}}$ as defined in Eq. (6). Note also that the description could be improved by considering the correction factors constituted by the higher order terms of the asymptotic process. These could be relevant in case scale separation is not fulfilled. The inner resonance effect appears in Eq. (8) through the frequency dependent effective parameter $\langle\phi_\omega\rangle$, associated with the dynamic motion of the internal plate. This results into a non conventional apparent mass term whose determination is performed by integrating the transverse displacement of the internal plate over its surface. Since there is no analytical expression of this quantity for a square clamped plate, the latter is approximated by that of a clamped circular plate. This provides an approximated value, denoted $\langle\phi^c_\omega\rangle$, for a square plate of side l by matching its first eigenfrequency with that of an equivalent circular plate of radius a. The corresponding approximation reads:

$$\langle\phi_\omega\rangle \approx \langle\phi^c_\omega\rangle = \frac{4}{\delta a}\frac{I_1(\delta a)J_1(\delta a)}{I_1(\delta a)J_0(\delta a) + I_0(\delta a)J_1(\delta a)} \tag{9}$$

where $a \approx 0.53l$ is the equivalent radius, J_k and I_k are the Bessel and modified Bessel functions of the first/second kind, δ is the wavenumber such that $\delta^4 = \Lambda'_p\omega^2/E'_pI_p$. The denominator of Eq. (9) is the transcendental equation whose roots δa are used to calculate the eigenfrequencies of the circular plate. The matching is performed on the first mode, and determines the radius of the equivalent circular plate, that is $a = 0.53l$. Although this reasoning is empirical and based on the resemblance of the first mode shapes of a square and circular plate, this estimate perfectly fits the first resonance but over-predicts the eigenfrequency of the second mode with an error of 5%. (see [23]).

The properties of $\langle\phi_\omega\rangle$ are such that $\langle\phi_\omega\rangle \to 1$ as $\delta \to 0$ which means that the effective mass is the real static mass, and $\langle\phi_\omega\rangle \to \pm\infty$ as $I_1(\delta a)J_0(\delta a) + I_0(\delta a)J_1(\delta a) = 0$, which roots corresponds to the plate's eigenfrequencies.

1.3.3. Dispersion features

Assuming an harmonic bending wave in the form $u(\mathbf{x}) = \exp(ik_\theta \mathbf{n}_\theta.\mathbf{x})$ propagating in the direction $\mathbf{n}_\theta = \cos\theta \mathbf{e_x} + \sin\theta \mathbf{e_y}$. Taking into account the facts that the terms associated with polar moments $\mathbf{J}^{\mathcal{G}}$ are of weak magnitude compared to the translational inertia, this term can be disregarded at the leading order. Consequently, the bending wavenumber $k_\theta(\omega)$ is given by :

$$k_\theta^4 \left(\frac{E_x I_x}{\ell_y} \cos^4\theta + \frac{E_y I_y}{\ell_x} \sin^4\theta + \left(\frac{G_x \mathcal{I}_x}{\ell_y} + \frac{G_y \mathcal{I}_y}{\ell_x} \right) \cos^2\theta \sin^2\theta \right) - \omega^2(\Lambda^{\mathcal{G}} + \Lambda'_p \langle \phi_\omega \rangle) = 0 \quad (10)$$

The inner resonance contained in $\langle \phi_\omega \rangle$ leads to dispersion features that differs distinctly from the classical bending case in which $k \propto \sqrt{\omega}$ in the whole frequency range. Significant changes are expected in the neighborhood of the internal plate's eigenmodes. Wavenumbers will be the subject of a special discussion in the section 2.1.

1.4. Concluding remarks

As an extension to the classical orthotropic plate equation Eq. (1) with coefficients Eq. (2) proposed by Timoshenko, homogenization introduces a dynamic description taking into account contrast between the beam and internal plates. Such an extended formulation is found as :

$$\frac{E_x I_x}{\ell_y} \frac{\partial^4 u}{\partial x^4} + \frac{E_y I_y}{\ell_x} \frac{\partial^4 u}{\partial y^4} + \left(\frac{G_x \mathcal{I}_x}{\ell_y} + \frac{G_y \mathcal{I}_y}{\ell_x} \right) \frac{\partial^4 u}{\partial x^2 \partial y^2} + \omega^2 \left(\frac{\rho_y J_y}{\ell_x} \frac{\partial^2 u}{\partial x^2} + \frac{\rho_x J_x}{\ell_y} \frac{\partial^2 u}{\partial y^2} \right) = \omega^2 (\Lambda^{\mathcal{G}} + \Lambda_p \langle \phi_\omega \rangle) u \quad (11)$$

Remarking that the terms associated with polar moments are of weak magnitude compared to the inertia, this term can be neglected at the leading order, so that Eq. (11) degenerates into

$$\left(D_x \frac{\partial^4}{\partial x^4} + D_y \frac{\partial^4}{\partial y^4} + 2 D_{xy} \frac{\partial^4}{\partial x^2 \partial y^2} \right) u = \omega^2 (\Lambda^{\mathcal{G}} + \Lambda_p \langle \phi_\omega \rangle) u \quad (12)$$

where the bending stiffness and mass are

$$D_x = \frac{E_x I_x}{\ell_y} \; ; \; D_y = \frac{E_y I_y}{\ell_x} \; ; \; D_{xy} = \frac{G_x \mathcal{I}_x}{\ell_y} + \frac{G_y \mathcal{I}_y}{\ell_x} \; ; \; \Lambda^{\mathcal{G}} = \frac{\Lambda_x}{\ell_y} + \frac{\Lambda_y}{\ell_x} \quad (13)$$

From Eq. (11) with coefficients Eq. (13), two important observations are made. First, the structure of the differential operation changes in such a way it still contains the bi-laplacian operator and includes additional terms of bending and torsional stiffness with rotational inertia. Second, the reference equation Eq. (1) with coefficients Eq. (2) no longer considers the plate contribution in the elastic part, but in the inertial part. The plate is no longer contained in the bending stiffness. This is fully consistent with the fact that a contrasted ribbed plate will exhibit a dynamic behavior mostly governed by the grid, and the internal plates will affect the global response only around frequency bands in which their dynamic behavior differs from that of the grid.

From this introduction on the mechanical part, the sound radiation from plates can be modeled assuming it is either infinite or finite. The next two sections 2 and 3 are respectively dedicated to infinite and finite cases.

2. Acoustic radiation - Infinite case

This section presents an investigation onto a infinite ribbed plate. In anticipation of an experimental investigation, the dimensions of the internal plates are calculated so as to correspond to a feasible plate. Two designs are obtained : first is denoted $\mathcal{R}_1^\infty$, and is associated with geometrical and mechanical contrast between the grid and internal plate considering the ribs are identical in the two directions, second is denoted $\mathcal{R}_2^\infty$, and introduces stiffeners of different dimensions in the two directions, in order to better exhibit the orthotropic nature of the plate. According to the indicators defined in section 2.1, as well as the geometrical parameters and mechanical properties given in Table 1, Table 2, the investigation will be expanded in terms of radiation efficiency (section 2.2) and transmission loss (section 2.3).

2.1. Methods and chosen sets of parameters

As for the methods, let consider an infinite plate with incident acoustic plane wave, as illustrated in Fig. 2. The expressions the transmission coefficient is derived from *i*) the acoustic pressure of the incident, reflected and transmitted waves, *ii*) the pressure difference on both face of the plate combined with *iii*) the continuity of pressure and velocity at the fluid-solid interface.

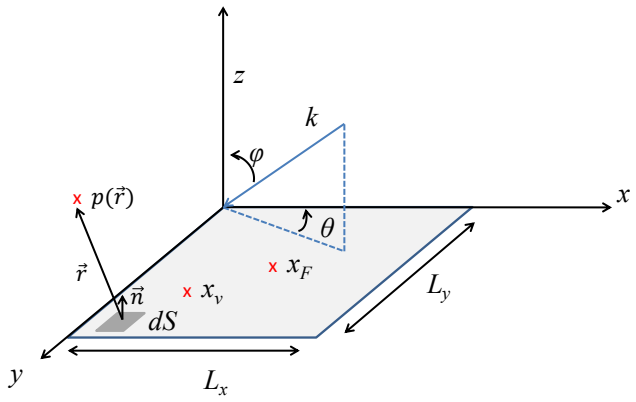

Figure 2: Notations used for the sound radiation investigation : ribbed plate in the (x, y) plane, angle of incident plane wave ϕ, azimuth angle θ of wave propagating in the plate. Location of point force x_F and observation point x_v for calculation of structural response. Elementary radiating surface dS with normal direction $\mathbf{n}$ towards receiver point.

Let us consider an infinite orthotropic plate driven by an incident pressure $p(x, y, z)$ which governing equation is :

$$\left(D_x \frac{\partial^4}{\partial x^4} + D_y \frac{\partial^4}{\partial y^4} + 2D_{xy} \frac{\partial^4}{\partial x^2 \partial y^2} \right) u - \omega^2 \Lambda u = p(x, y, z) \tag{14}$$

When the pressure field is supposed of the form of an incident plane wave with a wavenumber $k = \omega/c_0$, an incidence angle ϕ and an azimuth angle θ. In this case, the incidence angle ϕ is the angle between the wave vector and the normal direction to the plate, and the azimuth angle θ gives its orientation in the plane of the plate. As for the incident plane wave, we state $p(x, y, z)$ as:

$$p(x, y, z) = p_0 \exp(-i(k_x x + k_y y + k_z z)) \tag{15}$$

with $k_x = k \sin\phi \cos\theta$, $k_y = k \sin\phi \sin\theta$, $k_z = k \cos\phi$ are the acoustic wavenumbers in the different directions.

On the surface of the plate, $p(x, y, z = 0) = p_0 \exp(-i(k_x x + k_y y))$, the transverse displacement on the plate, solution of the equation Eq. (14) is searched with the form:

$$u(x, y) = U \exp(-ik \sin\phi(\cos\theta x + \sin\theta y)) \tag{16}$$

The ratio between the acoustic pressure to the velocity of the plate is introduced as the surface impedance $Z_s = p/v = p/i\omega u$.

The forms of the pressure and the displacement are the same as for the infinite isotropic plate but in case of orthotropic plate, due to the angle dependence of the flexural wavenumber k_p, the relation becomes

$$(D_x \cos^4\theta + D_y \sin^4\theta + 2D_{xy}\cos^2\theta\sin^2\theta)(k^4\sin^4\phi - k_p^4(\theta))u = p \qquad (17)$$

and therefore, the surface impedance is defined by:

$$Z_s(\theta,\phi) = \frac{-i}{\omega}\left(D_x \cos^4\theta + D_y \sin^4\theta + 2D_{xy}\cos^2\theta\sin^2\theta\right)\left(k^4\sin^4\phi - k_p^4(\theta)\right) \qquad (18)$$

Due to the orthotropic nature of plate, and thus the existence of two critical frequencies, the coincidence frequency band exhibiting a typical gap becomes broader and smoother. A relatively small difference between the bending rigidity of stiffeners produces a small difference between their respective critical frequencies. As the difference of stiffness increases, the critical frequencies might be separated by one or two orders of magnitude.

From this observation, the usual expression of surface impedance Z_s includes these two critical frequencies, whose depend not only on the angle of incidence ϕ of the incident plane wave, but also on the azimuth angle θ in the plane of the plate (see Fig. 2). The surface impedance of the orthotropic plate is thus :

$$Z_s = j\omega\Lambda\left(1 - \left(\frac{f}{f_{c,x}}\cos^2\theta + \frac{f}{f_{c,y}}\sin^2\theta\right)^2\sin^4\phi\right) \qquad (19)$$

For a given angle of incidence ϕ, the transmission coefficient τ is defined by :

$$\tau_{(\phi,\theta)} = \frac{1}{\left|\frac{Z_s}{2Z_0} + 1\right|^2} \qquad (20)$$

with $Z_0 = \rho_0 c_0/\cos\phi$ the normal impedance of the fluid and Z_s the surface impedance of the plate. The calculation of this transmission coefficient in diffuse field conditions is performed by integrating Eq. (20) over all angles of incidence. Assuming plane wave incidence uniformly distributed over all angles, the statistical transmission factor is :

$$\tau_d = \frac{2}{\pi}\int_0^{\pi/2}\left(2\int_0^{\pi/2}\tau_{(\phi,\theta)}\cos\phi\sin\phi\,\mathrm{d}\phi\right)\mathrm{d}\theta \qquad (21)$$

Introducing finally τ as Eq. (20), the diffuse field transmission coefficient is formulated as :

$$\tau_d = \frac{2}{\pi} \int_0^{\pi/2} \int_0^1 \frac{\mathrm{d}(\sin^2 \phi)\ \mathrm{d}\theta}{\left| \frac{Z_s}{2Z_0} + 1 \right|^2} \tag{22}$$

In the following, the evaluation of this term is performed numerically. In addition to the transmission coefficient, the reduction index R is introduced as $R = -10 \log(\tau_d)$.

According to the design rules favorable to inner resonance presented above and considering a feasibility criterion, two designs are obtained : first is denoted $\mathcal{R}_1^\infty$, and is associated with geometrical and mechanical contrast between the grid and internal plate considering the ribs are identical in the two directions, second is denoted $\mathcal{R}_2^\infty$, and introduces stiffeners of different dimensions in the two directions. The geometrical parameters and mechanical properties are respectively given in Table 1 and Table 2. The models use hysteretic damping ratio introduced as an imaginary part of the Young's modulus $E = E(1 + i\eta)$, with η =1% for aluminium and 5% for perspex.

Table 1: Geometrical parameters and mechanical properties associated with the 2D infinite ribbed plate $\mathcal{R}_1^\infty$.

$n_x = n_y = \infty$	E (GPa), ν	ρ (kg/m^3)	Dimensions (m)
Beam grid	E_b=69; $\nu_b = 0.3$	ρ_b=2700	$h_x = h_y = 1.5.10^{-2}$ $b_x = b_y = 1.5.10^{-2}$
Internal plates	E_p=2; $\nu_p = 0.37$	ρ_p=1200	$l_x = l_y = 7.10^{-2}$ $d = 3.10^{-3}$

Following the design $\mathcal{R}_1^\infty$ in Table 1, the exact critical frequency is the same in both directions $f_{c,j} = \frac{c^2}{2\pi}\sqrt{\frac{\lambda_j + \lambda_p D \langle \phi_\omega \rangle}{D_j}}$. The first resonance frequency of the internal plate is $f_1^r = 1386$ Hz.

Following the design $\mathcal{R}_2^\infty$ in Table 2, the exact critical frequencies in both directions $f_{c,j} = \frac{c^2}{2\pi}\sqrt{\frac{\lambda_j + \lambda_p D \langle \phi_\omega \rangle}{D_j}}$ could be estimated numerically. As an approximation, out of the inner resonance frequency bands, this critical

Table 2: Geometrical parameters and mechanical properties associated with the 2D infinite ribbed plate $\mathcal{R}_2^\infty$.

$n_x = n_y = \infty$	E (GPa), ν	ρ (kg/m^3)	Dimensions (m)
Beam grid	E_b=69; $\nu_b = 0.3$	ρ_b=2700	$h_x = 1.10^{-2}, h_y = 0.75.10^{-2}$
			$b_x = b_y = 1.10^{-2}$
Internal plates	E_p=2; $\nu_p = 0.37$	ρ_p=1200	$l_x = l_y = 7.6.10^{-2}$
			$d = 3.10^{-3}$

frequency is bounded by that of a simple plate radiating in half-space $f_c^- = \frac{c^2}{2\pi}\sqrt{\frac{\lambda_b}{D_x}}$, that is $f_c^- = 1613$ Hz as the lower bound, and will not be greater than that of the rib and internal plate at rest $f_{c,j}^+ = \frac{c^2}{2\pi}\sqrt{\frac{\lambda_j+\lambda_p}{D_j}}$, that is $f_{c,x}^+ = 2520$ Hz as the upper bound. This can be systematically verified. The same observation is valid for the other direction, respectively $f_{c,y}^- = 2520$ Hz, and $f_{c,y}^+ = 3323$ Hz. Also, the first resonance frequency of the internal plate is $f_1^r = 1190$ Hz, and the second resonance frequency is $f_2^r = 3261$ Hz.

The effective mass $\langle \phi_\omega \rangle$ associated to internal for both design is plotted in Fig. 3 for both designs. The trends observed is consistent with the behavior with the comment provided along Eq. (9), where the two resonance frequencies clearly appear.

From Fig. 4, it can be shown that due to inner resonance, the flexural wavenumber, calculated from Eq. (10), can significantly vary below and above the critical frequency. Classical results of acoustic radiation below and above the critical frequency can be obtained for 60 Hz and 900 Hz respectively. However, in case of inner resonance, the flexural wavelength can be significantly greater than acoustic wavelength below the critical frequency, giving rise to unconventional acoustic radiation. Alternatively, the flexural wavelength can be significantly lower than acoustic wavelength above the critical frequency, giving rise to unconventional generation of evanescent acoustic waves.

2.2. Radiation efficiency

An usual indicator to evaluate if a vibrating surface is a good sound radiator is the radiation efficiency denoted σ defined in terms of wavenumbers

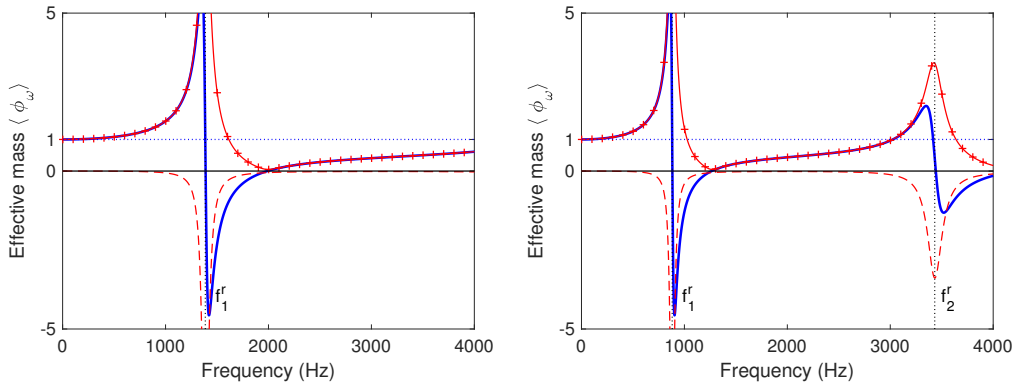

Figure 3: Dimensionless effective mass ϕ_ω associated with one single internal plate : real part $(-)$, imaginary part $(- -)$, modulus $(- + -)$, normalized static mass $y = 1$ $(\cdots)$. For plate $\mathcal{R}_1^\infty$ (a) and plate $\mathcal{R}_2^\infty$ (b).

as $\sigma = 1/\sqrt{1 - k_p^2/k^2}$. In this formula, we assume $k_p < k$; when the flexural wavelength in the plate increases with respect to the acoustic wavelength in air, the radiation efficiency tends to 1. The radiation efficiency is illustrated in Fig. 5 for both designs introduced above. As for the plate $\mathcal{R}_1^\infty$, for which stiffeners are identical in both directions, σ is the same for $\theta = 0$ or $\pi/2$, and the tuning of the inner resonance frequency onto the critical frequency decreases significantly the radiation factor in this region where the plate is known to be acoustically transparent. As for the plate $\mathcal{R}_2^\infty$, for which stiffeners are different in both directions, σ is illustrated for $\theta = 0$ and $\theta = \pi/2$ and the influence of resonance frequencies is exhibited.

Radiation efficiency is an indicator for observing a preliminary manifestation of the local resonance effect. It gives an indication of the behavior in the main directions of orthotropy. A global description obtained from an integration on all angles, in the plate and in the air is proposed in the following section.

2.3. Sound transmission loss

2.3.1. Results for a single incidence angle

Two incidence angle are considered here for the acoustic wave reaching the plate : normal incidence condition $\phi = 0$, oblique incidence condition $\phi = \pi/3$.

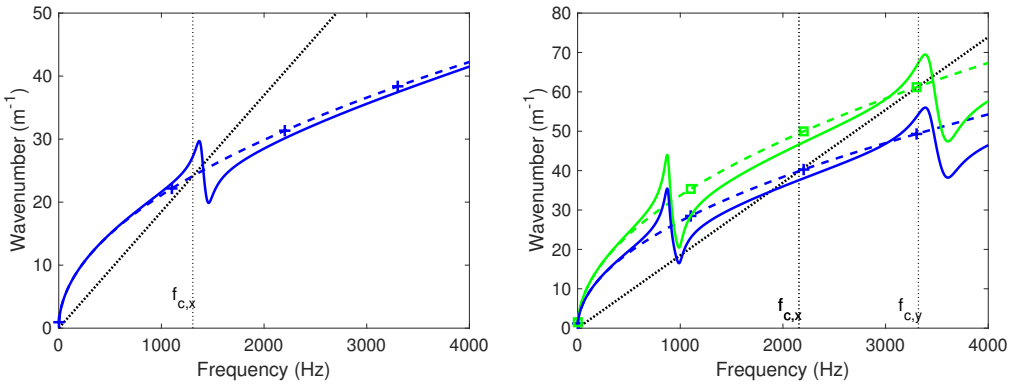

Figure 4: Flexural wavenumber in the $x-$ and $y-$ direction without inner resonance (resp. $(-+-)$ and $(-\square-)$) and with inner resonance (resp. $(-)$, $(-)$), acoustic wavenumber in air $(\cdots)$, and vertical dotted lines located at crossings indicated critical frequencies. For plate $\mathcal{R}_1^\infty$ (a) and plate $\mathcal{R}_2^\infty$ (b).

As for the normal incidence condition, Eq. (18) simplifies so as elastic effects vanish and only inertial effect remain, that is consistent with the mass law approximation, which gives a quite appropriate description for frequencies lower than the critical frequency. The normal incidence transmission loss is illustrated for the two design in Fig. 6.

As for the oblique incidence, an arbitrary angle for the propagating wave in the plate is chosen as $\theta = \pi/3$. After passing the coincidence frequency, the transmission loss exhibits strong frequency dependence and the bending stiffness (elastic effects) becomes predominant over the mass law. This effect is illustrated in Fig. 7 for 3 values of incidence angle, which shows that the classic trends are correctly recovered, *i.e.* the coincidence frequency decreases as the angle of incidence get closer to the grazing incidence, and that the introduction of local resonance is perceptible in specific interval without modified the change of slope below and above the coincidence frequency.

To extend these results to diffuse field, one may integrate over all possible incidence angles ϕ of the acoustic wave in air and possible directions of propagation θ of bending wave in the plate. The limits of the domains of integration are withdrawn since they correspond to grazing incidences and can give numerical errors.

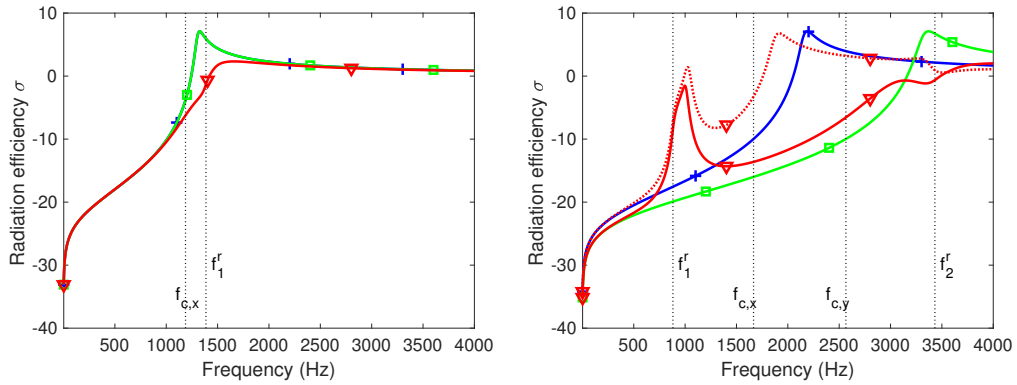

Figure 5: Radiation efficiency of orthotropic plate with inner resonance for $\theta = \pi/2$ ($-\triangledown-$), $\theta = 0$ ($\cdots\triangledown\cdots$), equivalent isotropic plate in $x-$ direction ($-+-$) and $y-$ direction ($-\square-$). For plate $\mathcal{R}_1^\infty$ (a) and plate $\mathcal{R}_2^\infty$ (b).

2.3.2. Results in diffuse field conditions

The transmission loss is now calculated for the two designs. For each design, the transmission loss of the plate considering inert internal plates and the plate with the dynamic of the internal plates is plotted to best evidence the local resonance.

As for the design of the ribbed plate $\mathcal{R}_1^\infty$ given in Table 1, the diffuse field transmission loss clearly shows the coincidence frequency of the equivalent isotropic plate in the $x-$ direction and the plate at rest. The small shift in coincidence frequency is due to the increase of mass. However the most noticeable effects lies in the increase of transmission loss around the coincidence frequency. Minor fluctuations visible at high frequency are due to the discretization of the angle interval and are not related with inner resonance.

As for the design of the ribbed plate $\mathcal{R}_2^\infty$ given in Table 2. Several quantities are illustrated, namely, the transmission loss associated with the equivalent isotropic plate along $x-$ and $y-$, that associated with the orthotropic plate without inner resonance (disabling the frequency dependent term in Eq. (11), that is $\langle\phi_\omega\rangle = 1$), and that including the local resonance. Comparison is shown in Fig. 8 and shows the two critical frequencies associated with the equivalent isotropic plates along $-x$ and $-y$, since these have different bending stiffness in the two directions. A relatively small difference between rigidities produces a small difference between critical frequencies. The ribs increase the bending stiffness but lowers the critical frequency. This may

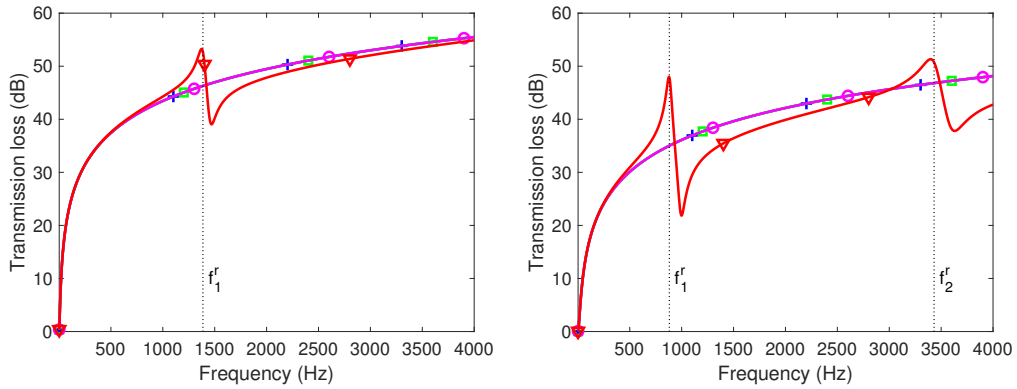

Figure 6: Normal incidence transmission loss of orthotropic plate with inner resonance ($-\bigtriangledown-$), plate at rest ($-\bigcirc-$), equivalent isotropic plate in $x-$ direction ($-+-$) and $y-$ direction ($-\square-$). For plate $\mathcal{R}_1^\infty$ (a) and plate $\mathcal{R}_2^\infty$ (b).

lead to an increased transparency in the useful frequency range. However, the locally resonant nature can be put to good use since it provides an additional mechanism of attenuation in some frequency bands. In this way, the transmission loss of the orthotropic plate exhibits a dip between the aforementioned critical frequencies. When introducing the resonance of internal plates, additional fluctuations related to eigenmodes of the vibrating internal plates contribute to the increase or decrease of transmission loss at their corresponding frequencies.

2.4. Concluding remarks on infinite case

This section introduced the relevant quantities to look at when investigating the radiation of plates Two realistic designs are obtained : first is associated with geometrical and mechanical contrast between the grid and internal plate, second introduces different stiffeners in the two directions, in order to better exhibit the orthotropic nature of the plate, still with inner resonance. Preliminary examination of wavenumbers suggests that in case of inner resonance, the flexural wavelength can be greater than the acoustic wavelength below the critical frequency, giving rise to acoustic radiation, and alternatively, it can be lower than acoustic wavelength above the critical frequency, giving rise to unconventional generation of evanescent acoustic waves. This is then confirmed by the observation of radiation efficiency, which shows that tuning the inner resonance frequency around the critical

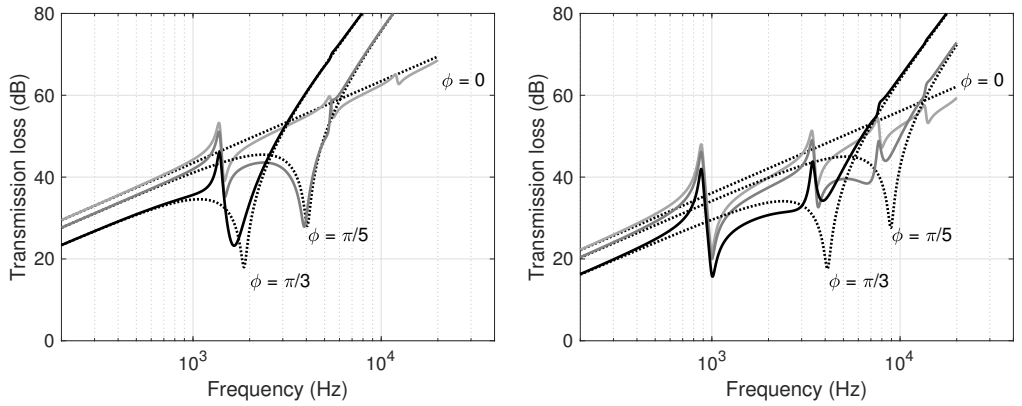

Figure 7: Oblique incidence transmission loss of orthotropic plate with inner resonance (–), plate at rest $(\cdots)$, for $\phi = 0, \pi/5, \pi/3$, from light to dark grey. For plate $\mathcal{R}_1^\infty$ (a) and plate $\mathcal{R}_2^\infty$ (b).

frequency leads to significant attenuation. Finally, exploring the trends of transmission loss in either single incidence angle or diffuse field shows that the locally resonant nature of the plate bring additional attenuation in the coincidence region where the plate is known to be acoustically transparent.

3. Acoustic radiation - Finite case

The previous designs $\mathcal{R}_1^\infty$ and $\mathcal{R}_2^\infty$ are supplemented by finite dimensions $L_x = L_y = 0.7$ m, and are denoted $\mathcal{R}_1$ and $\mathcal{R}_2$. $\mathcal{R}_1$ has $n_x = n_y = 8$ cells, $\mathcal{R}_2$ has $n_x = n_y = 7$ cells. For explanatory purposes and in order to demonstrate the effect of locally resonant nature of the plate on the sound transmission loss, the simply supported case is chosen since it offers an analytical solution in the form of a double summation of sine terms. The location of point force and observation point for calculation of structural response are sketched in Fig. 2. From this setup, structural frequency response functions are assessed in section 3.1, then mean square velocity is commented in section 3.2. The behaviors identified make it possible to better understand the shape of the transmission loss curve in section 3.3.

3.1. Comparison of Timoshenko and homogenized model

This section briefly presents the structural response of the orthogonally ribbed plate modeled either with Timoshenko equation Eq. (1) or homog-

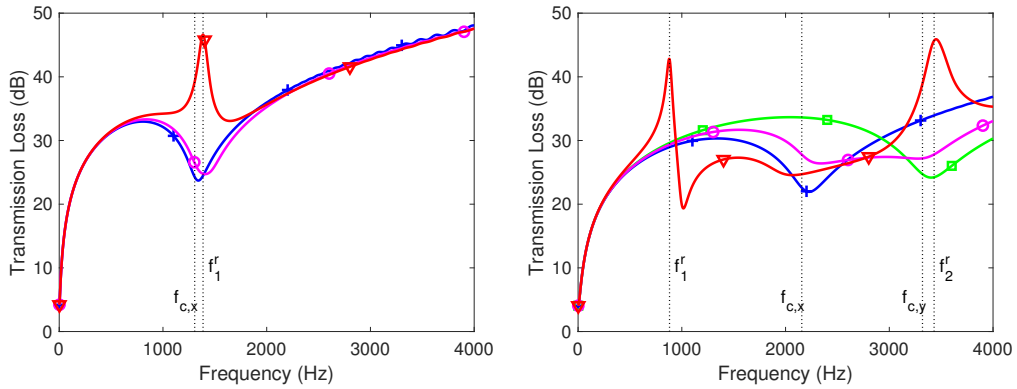

Figure 8: Diffuse field transmission loss of orthotropic plate with inner resonance ($-\,\triangledown\,-$), plate at rest ($-\,\bigcirc\,-$), equivalent isotropic plate in $x-$ direction ($-\,+\,-$) and $y-$ direction ($-\square-$). For plate $\mathcal{R}_1^\infty$ (a) and plate $\mathcal{R}_2^\infty$ (b).

enized model with inner resonance Eq. (11). For this purpose, a structural point force is located at coordinates $x_F = (L_x/2, L_y/2)$ and the transverse velocity is calculated at a virtual observation point with coordinates $x_v = (L_x/3, L_y/3)$. In this way, the structural frequency response function defined as the ratio of velocity versus input force, namely mobility $M(\omega) = i\omega u/F$, is calculated analytically. For the sake of simplicity, plates with simply supported boundary conditions all around are considered since there are distinct solutions for the wavenumbers k_x and k_y and it provides an analytical solution. The solution for the transverse displacement field $u(x, y, \omega)$ is formulated as the infinite sum of all possible solutions $u(x, y, \omega) = \sum_{m=1}^{\infty}\sum_{n=1}^{\infty} u_{m,n}(\omega)\Psi_{m,n}(x, y)$, where $\Psi_{m,n}(x, y)$ is the (m, n) mode shape function and $w_{m,n}(\omega)$ the associated amplitude. In case of a plate supported along all four edges, the modal functions are $\Psi_{m,n}(x, y) = \sin(m\pi x/L_x)\sin(n\pi y/L_y)$. This modal summation technique can be approximated as a finite sum as $u(x, y, \omega) \approx \sum_{m=1}^{M}\sum_{n=1}^{N} u_{m,n}(\omega)\Psi_{m,n}(x, y)$, where M and N are the number of modes considered. Considering 50 modes, the computational time is about 4 seconds and associated results are given for both designs on Fig. 9. The structural mobility is calculated as

Apart from the inner resonance frequencies specific to each design, the very low frequency behavior is well captured by the homogenized model, as well as the trend in rather high frequency domain. In addition, the response

from homogenized model exhibits proper drops of amplitude at the frequencies identified as inner resonance frequencies, which makes it possible to rely on its ability to predict local phenomena.

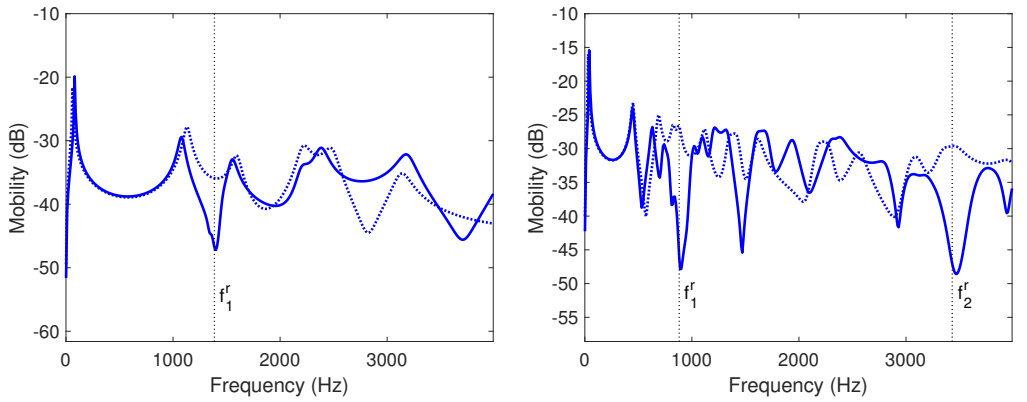

(a) (b)

Figure 9: Structural mobility (ref:1m/s/N) of simply supported orthotropic plate with inner resonance computed analytically from homogenized model (−) and Timoshenko model (···). For plate $\mathcal{R}_1$ (a) and plate $\mathcal{R}_2$ (b).

3.2. Effect on mean square velocity

The mean square velocity is a structural indicator of the radiation performance, it is defined as the quadratic normal component of the structural velocity integrated over the surface of the plate S as $\tilde{v} = \sqrt{1/S \int_S |i\omega u|^2}$. The mean square velocity is calculated from this expression for both designs with same location of excitation point as in the previous section 3.1.

As illustrated in Fig. 10, the global modes are correctly predicted by the two models, especially in the low frequency region. However, strong disparity appears around the inner resonance frequencies, and the homogenized model shows better capability in predicting the gap induced by local resonance. Indeed, it is derived as a beam grid enriched by local motion of internal plates. As contrast between beam grid and plate constituents increases, the amplitude of motion experienced by internal plates becomes much different than that of the beam grid, leading to a poorer accuracy of Timoshenko model and giving advantage to the homogenized model.

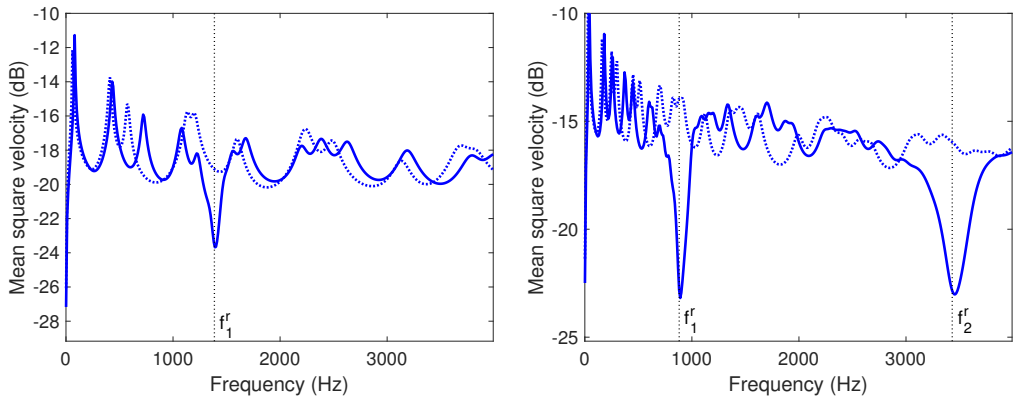

Figure 10: Mean square velocity (ref:1m/s/N) of orthotropic plate with inner resonance computed analytically from homogenized model (–) and Timoshenko model (···). For plate $\mathcal{R}_1$ (a) and plate $\mathcal{R}_2$ (b).

3.3. Effect on transmission loss

The transmission loss is here investigated by supplementing the previous model with simply supported plate. As for the structural part, the input vibratory field is the the same as the one calculated in section 3.1. As for the acoustic part, the notations are indicated in Fig. 2. The Rayleigh integral is implemented as it is known to be an efficient basis to calculate sound radiation from finite sized plane surface set into an infinite rigid baffle. The infinite baffle simplifies the general Helmholtz formulation so that only one integral is left, and the acoustic pressure is :

$$p(\mathbf{r},\omega) = \frac{j\omega\rho}{2\pi}\iint_S \frac{v_n(\mathbf{r_S})\exp(-ikR)}{R}\,\mathrm{d}S \tag{23}$$

where $v_n(\mathbf{r_S})$ is the normal velocity field over the surface, k is the acoustic wavenumber and $R = \|\mathbf{r_S} - \mathbf{r}\| = \sqrt{(x-x')^2 + (y-y')^2 + z'^2}$ is the distance between each elementary source point on the plate $\mathbf{r_S} = (x, y, 0)$ and the receiver point $\mathbf{r} = (x', y', z')$. The sources are defined by subdividing the plate into a regular grid of 100×100 elementary sources. For the calculation of transmission loss, $z' << 1$.

The results in terms of sound transmission loss are represented in Fig. 11. Since our phenomenon occurs in a narrow interval, the choice is made not to adopt the classical representation in third octave bands. For both plates,

we see that inner resonance introduces additional loss in the sound transmission To best emphasize the locally resonant feature, it is compared as in Fig. 10 with the Timoshenko model to show the interval of differences. The homogenized model is also used with internal plates at rest, which does not correspond to a physical case but associated with a asymptotic behavior.

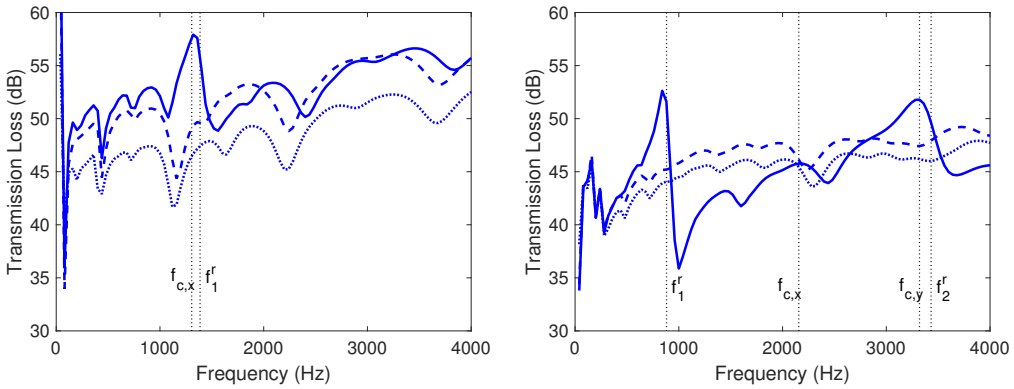

Figure 11: Transmission loss estimated analytically in case of finite plate, from homogenized model with resonant plates (−), homogenized with plates at rest (− −), and from Timoshenko model (···). For plate $\mathcal{R}_1$ (a) and plate $\mathcal{R}_2$ (b).

Conclusion

Based on explicit design rules and homogenized plate model, this paper brings phenomenological interpretation on the radiation of ribbed plates, and specifically focuses on the parallel between an homogenized analytical model of contrasted ribbed and its acoustic radiation compared to the Timoshenko orthotropic plate model. For ribbed plates with strong contrasts between constituents, it is firstly demonstrated that this model supplements Timoshenko model. The latter is suitable for ribbed plates in which the rigidity of the plate is introduced in the bending stiffness of the ribs, whereas the homogenized model can be seen as a beam grid whose dynamic behavior is corrected by the motion of vibrating internal plates. Investigations of the acoustic radiation from an infinite and finite orthogonally ribbed plate are based on two designs associated with strong and low contrast between constituents, in order to better exhibit the orthotropic nature of the plate.

As a preliminary comprehensive study case, the infinite plate case is presented. The limit behavior of equivalent isotropic plates in the two directions of orthotropy are successfully identified. The radiation efficiency exhibits the transition from non-radiating to radiating domains marked out by the critical frequency. The effect of the local resonance is also evidenced and results in an unconventional increase or reduction of the radiation below or above the critical frequency.

As a complementary case, analytical predictions of mean square velocity and transmission loss are commented for finite plates. It comes out that the homogenized provides enhanced estimation of behavior in inner frequency ranges compared to Timoshenko model. The examination of the sound transmission loss demonstrates the attenuation in the neighborhood of inner resonance.

Although the homogenization process could be further applied on various cell geometries, this paper specifically outlines the relevancy of the homogenized model and demonstrates its ability to predict acoustic radiation of contrasted plates. The large amount of possible setups suggest adjustable resonant properties of the panel behavior, and offers the possibility of either broadband or narrow band attenuation.

CRediT author statement

Pascal Fossat: Conceptualization, Methodology, Software, Writing - original draft, Writing - review & editing. **Thomas Brion**: Methodology, Software, Writing - review & editing. **Mohamed Ichchou**: Conceptualization, Writing - review & editing, Validation, Project administration, Funding acquisition. **Olivier Bareille**: Supervision, Project administration, Funding acquisition.

Acknowledgments

This work was supported by the LabEx CeLyA (Centre Lyonnais d' Acoustique, ANR-10-LABX-0060) of Université de Lyon, within the program "Investissements d'Avenir" (ANR-11-IDEX-0007) operated by the French National Research Agency (ANR).

References

[1] P. W. Smith, Coupling of sound and panel vibration below the critical frequency, The Journal of the Acoustical Society of America 36 (8) (1964) 1516–1520. arXiv:https://doi.org/10.1121/1.1919235, doi:10.1121/1.1919235.
URL https://doi.org/10.1121/1.1919235

[2] N. Lomas, S. Hayek, Vibration and acoustic radiation of elastically supported rectangular plates, Journal of Sound and Vibration 52 (1) (1977) 1–25. doi:https://doi.org/10.1016/0022-460X(77)90385-6.
URL https://www.sciencedirect.com/science/article/pii/0022460X77903856

[3] A. Berry, J. Nicolas, Structural acoustics and vibration behavior of complex panels, Applied Acoustics 43 (3) (1994) 185–215, structural Acoustics and Vibrations. doi:https://doi.org/10.1016/0003-682X(94)90047-7.
URL https://www.sciencedirect.com/science/article/pii/0003682X94900477

[4] N. Atalla, R. Bernhard, Review of numerical solutions for low-frequency structural-acoustic problems, Applied Acoustics 43 (3) (1994) 271–294, structural Acoustics and Vibrations. doi:https://doi.org/10.1016/0003-682X(94)90050-7.
URL https://www.sciencedirect.com/science/article/pii/0003682X94900507

[5] E. Reynders, C. Van Hoorickx, A. Dijckmans, Sound transmission through finite rib-stiffened and orthotropic plates, Acta Acustica united with Acustica 102 (6) (2016) 999–1010. doi:https://doi.org/10.3813/AAA.919015.

[6] C. Decraene, G. Lombaert, E. P. Reynders, Prediction of diffuse sound transmission through finite-sized periodic structures, Journal of Sound and Vibration 528 (2022) 116851. doi:https://doi.org/10.1016/j.jsv.2022.116851.

[7] S. Timoshenko, S. Woinowsky-Krieger, Theory of Plates and Shells, Engineering mechanics series, McGraw-Hill, 1959.

[8] G. Maidanik, Response of ribbed panels to reverberant acoustic fields, The Journal of the Acoustical Society of America 34 (6) (1962) 809–826. arXiv:https://doi.org/10.1121/1.1918200, doi:10.1121/1.1918200.
URL https://doi.org/10.1121/1.1918200

[9] D. Crighton, G. Maidanik, Acoustic and vibration fields generated by ribs on a fluid-loaded panel, I: Plane-wave problems for a single rib, Journal of Sound and Vibration 75 (3) (1981) 437–452. doi:https://doi.org/10.1016/0022-460X(81)90388-6.
URL https://www.sciencedirect.com/science/article/pii/0022460X81903886

[10] B. Mace, Sound radiation from a plate reinforced by two sets of parallel stiffeners, Journal of Sound and Vibration 71 (3) (1980) 435–441. doi:https://doi.org/10.1016/0022-460X(80)90425-3.
URL https://www.sciencedirect.com/science/article/pii/0022460X80904253

[11] D. Mead, Y. Yaman, The harmonic response of rectangular sandwich plates with multiple stiffening: A flexural wave analysis, Journal of Sound and Vibration 145 (3) (1991) 409–428. doi:https://doi.org/10.1016/0022-460X(91)90111-V.
URL https://www.sciencedirect.com/science/article/pii/0022460X9190111V

[12] D. Mead, A general theory of harmonic wave propagation in linear periodic systems with multiple coupling, Journal of Sound and Vibration 27 (2) (1973) 235–260. doi:https://doi.org/10.1016/0022-460X(73)90064-3.
URL https://www.sciencedirect.com/science/article/pii/0022460X73900643

[13] J.-L. Christen, M. Ichchou, A. Zine, B. Troclet, Wave finite element formulation of the acoustic transmission through complex infinite plates, Acta Acustica united with Acustica 102 (6) (2016) 984–991. doi:https://doi.org/10.3813/AAA.919013.

[14] C. Droz, C. Zhou, M. Ichchou, J.-P. Lainé, A hybrid wave-mode formulation for the vibro-acoustic analysis of 2D periodic

649 structures, Journal of Sound and Vibration 363 (2016) 285–302.
650 doi:https://doi.org/10.1016/j.jsv.2015.11.003.
651 URL https://www.sciencedirect.com/science/article/pii/
652 S0022460X15008779

653 [15] F. Fahy, E. Lindqvist, Wave propagation in damped, stiff-
654 ened structures characteristic of ship construction, Journal of
655 Sound and Vibration 45 (1) (1976) 115–138. doi:https:
656 //doi.org/10.1016/0022-460X(76)90671-4.
657 URL https://www.sciencedirect.com/science/article/pii/
658 0022460X76906714

659 [16] J. Legault, A. Mejdi, N. Atalla, Vibro-acoustic response of or-
660 thogonally stiffened panels: The effects of finite dimensions,
661 Journal of Sound and Vibration 330 (24) (2011) 5928–5948.
662 doi:https://doi.org/10.1016/j.jsv.2011.07.017.
663 URL https://www.sciencedirect.com/science/article/pii/
664 S0022460X11005852

665 [17] H. Zhou, Y. Zhao, H. Wu, J. Meng, The vibroacoustic analysis of
666 periodic structure-stiffened plates, Journal of Sound and Vibration 481
667 (2020) 115402. doi:https://doi.org/10.1016/j.jsv.2020.115402.
668 URL https://www.sciencedirect.com/science/article/pii/
669 S0022460X20302340

670 [18] E. Sánchez-Palencia, Non-homogeneous media and vibration theory,
671 Lecture notes in physics 127.

672 [19] C. Chesnais, C. Boutin, S. Hans, Effects of the local resonance on
673 the wave propagation in periodic frame structures: Generalized new-
674 tonian mechanics, The Journal of the Acoustical Society of Amer-
675 ica 132 (4) (2012) 2873–2886. arXiv:https://doi.org/10.1121/1.
676 4744975, doi:10.1121/1.4744975.
677 URL https://doi.org/10.1121/1.4744975

678 [20] C. Boutin, K. Viverge, Generalized plate model for highly contrasted
679 laminates, European Journal of Mechanics - A/Solids 55 (2016) 149–
680 166. doi:https://doi.org/10.1016/j.euromechsol.2015.08.008.
681 URL https://www.sciencedirect.com/science/article/pii/
682 S0997753815001084

[21] K. Viverge, C. Boutin, F. Sallet, Model of highly contrasted plates versus experiments on laminated glass, International Journal of Solids and Structures 102-103 (2016) 238–258. doi:https://doi.org/10.1016/j.ijsolstr.2016.09.035.
URL https://www.sciencedirect.com/science/article/pii/S0020768316302840

[22] P. Fossat, C. Boutin, M. Ichchou, Dynamics of periodic ribbed plates with inner resonance: Analytical homogenized model and dispersion features, International Journal of Solids and Structures 152-153 (2018) 85–103. doi:https://doi.org/10.1016/j.ijsolstr.2018.06.012.
URL https://www.sciencedirect.com/science/article/pii/S0020768318302440

[23] C. Boutin, P. Fossat, C. Droz, M. Ichchou, Dynamics of ribbed plates with inner resonance: Analytical homogenized models and experimental validation, European Journal of Mechanics - A/Solids 79 (2020) 103838. doi:https://doi.org/10.1016/j.euromechsol.2019.103838.
URL https://www.sciencedirect.com/science/article/pii/S0997753819301664

[24] P. Fossat, M. Ichchou, Sound radiation of locally resonant unidirectionally ribbed plates, in: ASME 2021 International Mechanical Engineering Congress and Exposition, Vol. 85543, American Society of Mechanical Engineers, 2021. arXiv:https://asmedigitalcollection.asme.org/IMECE/proceedings-pdf/IMECE2021/85543/V001T01A032/6826596/v001t01a032-imece2021-70987.pdf, doi:10.1115/IMECE2021-70987.
URL https://doi.org/10.1115/IMECE2021-70987

[25] Z. Liu, R. Rumpler, L. Feng, Broadband locally resonant metamaterial sandwich plate for improved noise insulation in the coincidence region, Composite Structures 200 (2018) 165–172. doi:https://doi.org/10.1016/j.compstruct.2018.05.033.
URL https://www.sciencedirect.com/science/article/pii/S0263822318303520

[26] T. Yamamoto, Acoustic metamaterial plate embedded with helmholtz resonators for extraordinary sound transmission loss, Journal of Applied

Physics 123 (21) (2018) 215110. arXiv:https://doi.org/10.1063/1.5025570, doi:10.1063/1.5025570.
URL https://doi.org/10.1063/1.5025570

[27] C. Droz, O. Robin, M. Ichchou, N. Atalla, Improving sound transmission loss at ring frequency of a curved panel using tunable 3D-printed small-scale resonators, The Journal of the Acoustical Society of America 145 (1) (2019) EL72–EL78. arXiv:https://doi.org/10.1121/1.5088036, doi:10.1121/1.5088036.
URL https://doi.org/10.1121/1.5088036

[28] F. Errico, M. Ichchou, S. De Rosa, F. Franco, O. Bareille, Investigations about periodic design for broadband increased sound transmission loss of sandwich panels using 3D-printed models, Mechanical Systems and Signal Processing 136 (2020) 106432. doi:https://doi.org/10.1016/j.ymssp.2019.106432.
URL https://www.sciencedirect.com/science/article/pii/S0888327019306533